JOURNAL OF AGRICULTURAL AND FOOD CHEMISTRY

Article

pubs.acs.org/JAFC

Metabolic Survey of Defense Responses to a Compatible Hemibiotroph, *Phytophthora parasitica* var. *nicotianae*, in Ethylene Signaling-Impaired Tobacco

Kyoungwon Cho,[†] Yuran Kim,[†] Soo jin Wi,[§] Jong Bok Seo,[†] Joseph Kwon,[#] Joo Hee Chung,[†] Ky Young Park,[§] and Myung Hee Nam*[,†]

[†]Seoul Center, Korea Basic Science Institute (KBSI), Seoul 136-713, Republic of Korea

[§]Department of Biology, Sunchon National University, Sunchon, Chonnam 540-742, Republic of Korea

[#]Kwangju Center, Korea Basic Science Institute (KBSI), Kwangju 305-806, Republic of Korea

Supporting Information

ABSTRACT: Reactive oxygen species (ROS) and ethylene play an important role in determining the resistance or susceptibility of plants to pathogen attack. A previous study of the response of tobacco cultivar (*Nicotiana tabacum* L. cv. Wisconsin 38) to a compatible hemibiotroph, *Phytophthora parasitica* var. *nicotianae* (*Ppn*) showed that biphasic bursts of ROS and ethylene are positively associated with disease severity. The levels of ethylene and ROS might influence the susceptibility of plants to pathogens, with changing levels of metabolite related to disease resistance or susceptibility. In this study, to obtain more detailed information on the interaction of ROS and ethylene signaling related to resistance and/or susceptibility of plants to pathogen, *Ppn*-induced metabolic profiles from wild type (WT) and ethylene signaling-impaired transgenic plants that expressed *Ein3* antisense (*Ein3-AS*) were compared using ultraperformance liquid chromatography−quadrupole time-of-flight mass spectrometry (UPLC-QTOF-MS). Nonredundant mass ions (576 in ESI+ mode and 336 in ESI− mode) were selected, and 56 mass ions were identified on the basis of their accurate mass ions and MS/MS spectra. Two-way hierarchical clustering analysis of the selected mass ions revealed that nicotine and phenylpropanoid−polyamine conjugates, such as caffeoyl-dihydrocaffeoyl−spermidine, dicaffeoyl−spermidine, caffeoyl-feruloyl−spermidine, and two bis(dihydrocaffeoyl)−spermine isomers, and their intermediates, such as arginine and putrecine, were present at lower levels in *Ein3-AS* transgenic plants during *Ppn* interaction than in WT, whereas galactolipid and oxidized free fatty acid levels were higher in *Ein3-AS* transgenic plants. Taken together, these results reveal a function for ethylene signaling in tobacco defense responses during *Ppn* interaction.

KEYWORDS: *Nicotiana tabacum, metabolomics, UPLC-QTOF-MS, ethylene, ROS, compatible pathogen*

INTRODUCTION

Defense responses to pathogens in plants are initiated upon the recognition of pathogen attack. A rapid and transient production of reactive oxygen species (ROS), known as an oxidative burst, is one of the initial responses that follow successful recognition of diverse pathogens.[1] ROS are produced by (1) plasma-membrane-localized respiratory burst oxidase homologues (Rboh), referred to as NAD(P)H oxidases, which generate superoxide, in the plant apoplast[2,3] and (2) cell wall-localized peroxidases that generate hydrogen peroxide.[4] Different plant−pathogen interactions induce different patterns of ROS production. First, a transient and nonspecific accumulation of ROS occurs in both compatible and incompatible plant−pathogen interactions, but a second and prolonged oxidative burst at 4−9 h preferentially occurs in incompatible interactions and is associated with the establishment of the hypersensitive response (HR).[3−7] ROS not only have direct antimicrobial effects but also act as signaling molecules that induce defense responses, including accumulation of phytoalexins and expression of pathogen-related genes and HR.[5,7−11] Recent studies have shown that ROS are also associated with other signaling molecules, including ethylene.[9] Mur et al.[12] reported a biphasic production of ethylene in tobacco after inoculation with HR-eliciting *Pseudomonas syringae* pathovars. Similar to the biphasic ROS burst, the first increase in ethylene occurs in all interactions with HR-eliciting, disease-forming, and nonpathogenic strains. The second increase of ethylene relates to the HR formation. Co-treatment of tobacco leaves with a nitric oxide synthase inhibitor and an avirulent strain, *P. syringae* pv. *phaseolicola*, reduces the second ethylene increase and HR formation. Interaction between ROS and ethylene signaling was also suggested in large-scale analyses of gene expression in *Arabidopsis* and tobacco.[13,14] In these studies, ethylene-responsive elements and other genes involved in ethylene signaling were increased upon exogenous application of H_2O_2, indicating a link between ROS and ethylene responses. Ethylene has a critical role in H_2O_2 release during programmed cell death induced by camptothecin, a topoisomerase-I inhibitor, in tomato suspension cells.[15]

As for HR, ROS-induced programmed cell death is an effective defense mechanism against biotrophic pathogens that

Received: April 23, 2013
Revised: July 15, 2013
Accepted: July 18, 2013
Published: July 18, 2013

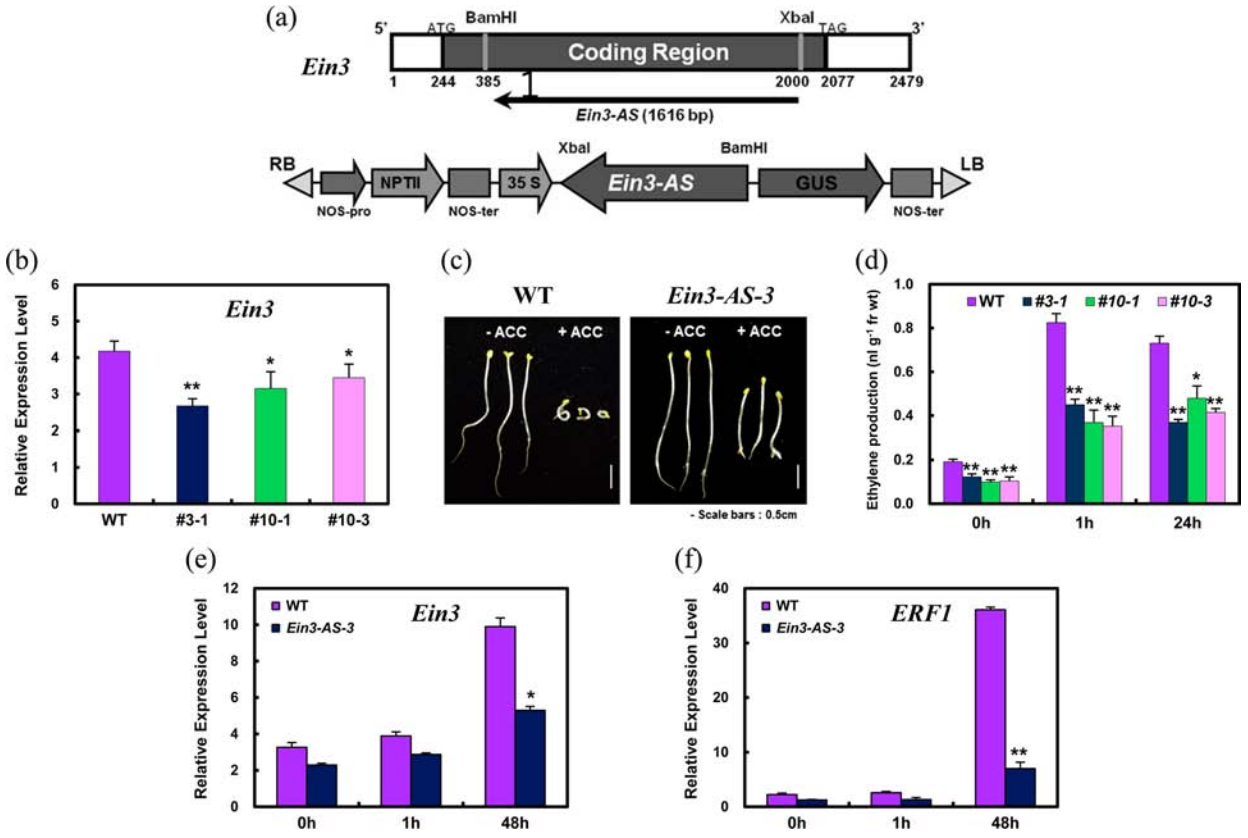

Figure 1. RT-PCR and phenotypic analysis of transgenic plants expressing Ein3 antisense: (a) construction of the *35S::Ein3* antisense chimeric construct; (b) basal levels of endogenous *Ein3* transcripts in leaf; (c) ethylene production; (d) triple-response phenotype of 10-day-old etiolated seedlings grown on MS medium supplemented with (+ACC) or without (−ACC) 10 μM ACC; (e, f) relative mRNA levels of *Ein3* and *ERF1* genes infected with *Ppn*. An asterisk indicates a significant difference between wild type and transgenic plants under *Ppn*-treated or untreated conditions. Data are statistically significant at *, $P < 0.1$; **, $P < 0.05$; or *** $P < 0.01$.

derive nutrients from living cells, but not against necrotrophic pathogens that derive nutrients from dead cells. In the case of necrotrophs, the induction of cell death in the host can be an important stimulus for virulent proliferation.[16] Preinfection of an avirulent strain leads to HR, thus enhancing the growth of a necrotroph, *Botrytis cinerea*. Moreover, inhibition of HR leads to enhanced resistance to *B. cinerea*.[17] Recently, our research group reported biphasic ROS and ethylene bursts after inoculation of a susceptible tobacco cultivar (*Nicotiana tabacum* L. cv. Wisconsin 38) with a compatible hemibiotroph, *Phytophthora parasitica* var. *nicotianae* (*Ppn*).[3] First, transient accumulation (phase I) of ROS and ethylene occurred at 1 and 3 h postpathogen inoculation (hpi), respectively, and a second massive burst (phase II) occurred at 48 and 72 hpi, respectively, followed by extensive cell death and pathogen proliferation. The biphasic ROS production was inhibited in transgenic plants expressing antisense to 1-aminocyclopropane-1-carboxylic acid (ACC) synthase, ACC oxidase, or homologue of ethylene insensitive3 (Ein3), as well as in transgenic plants impaired in ROS production. All of these transgenic plants represented increased tolerance to *Ppn*, too. The protective effects against *Ppn* progression were related to the synergistic inhibition of the second phase of ROS and ethylene production, suggesting that the levels of ethylene and ROS are correlated with compatible pathogen proliferation in susceptible plants.

LC-MS-based profiling of metabolites was used to identify a large set of resistance-related metabolites belonging to phenylpropanoid, flavonoid, fatty acid, and terpenoid metabolic pathways in barley subjected to Fusarium head blight.[18] Our previous study of nontargeted metabolite profiling in *Ppn*-treated tobacco revealed that a large set of resistance-related metabolites belonging to amino acids, phenylpropanoid, fatty acid, and phospholipids were changed by the compatible pathogen at each phase of ROS burst, reflecting the host responses attempting to block pathogen penetration.[19] The degree of change of metabolite may be an important factor to determine compatibility with the pathogen. The levels of ethylene and ROS might influence the degree of change of defense-related metabolite, influencing the susceptibility of plant to pathogen. However, how the biphasic production of ROS and ethylene mediates plant defense responses to *Ppn* is still unknown. In this study, as an effort to elucidate the interactive function of ROS and ethylene on the resistance and/or susceptibility of plant to pathogen, we applied metabolic profiling in wild type (WT) and ethylene signaling-impaired transgenic tobacco, which is more tolerant to *Ppn* than WT. Metabolite profiling using ultraperformance liquid chromatography−quadrupole time-of-flight mass spectrometry (UPLC-QTOF-MS) was applied at the first (1 hpi) and the second (48 hpi) bursts of ROS. Phenylpropanoid−polyamine conjugates and their intermediates were present at lower levels in *Ein3-AS* transgenic plants during *Ppn* interaction than in WT, whereas galactolipid and oxidized free fatty acid levels were higher in *Ein3-AS* transgenic plants. On the basis of the functions of the identified metabolites and their quantitative change in WT and

transgenic plant at each phase of *Ppn*-induced ROS burst, this paper investigated the interactive effect of ROS and ethylene signaling on the metabolic responses associated with defense and/or susceptible responses of tobacco to *Ppn*.

MATERIALS AND METHODS

Chemicals, Plants, and Pathogen Inoculation. Standard compounds, such as amino acids, phenolic compounds, lipids, and plant hormones (Olchemim Ltd.), including 1-aminocycloprophane-1carboylic acid (ACC), indole-3-acetic acid (IAA), *cis*-12-oxophytodienoic acid (OPDA), and (+)-*cis*,*trans*-abscisic acid (ABA), were utilized as previously mentioned.[19] Transgenic tobacco plants (*N. tabacum* L. cv. Wisconsin 38) were generated using constructs that consisted of a cauliflower mosaic virus 35S promoter and an *Ein3* antisense coding sequence, which were expressed via *Agrobacterium tumefaciens*-mediated gene transfer. A fragment (1616 bp) that corresponded to nucleotides 385−2000 of *Ein3* cDNA (*TEIL1*, GenBank accession no. AB015855) was subcloned into the binary vector pBI121 with an antisense orientation (Figure 1a). The expression of transgenes in kanamycin-resistant plants was verified by quantitative real-time PCR (Figure 1b). The triple-response phenotype was scored in T2 seedlings originating from individual kanamycin-resistant T1 plants. Fungal culture and inoculation were performed as described previously.[3]

RNA Isolation and Quantitative Real-Time PCR. Total RNA isolation and quantitative real-time PCR (qRT-PCR) were performed as described previously.[3] To analyze the relative abundance of transcripts by quantitative real-time PCR, 1 mg of total RNA from the leaf disks was reverse transcribed for 30 min at 42 °C in a 20 μL reaction volume using a High Fidelity PrimeScript RT-PCR kit (Takara). Real-time qRT-PCR was performed in optical 96-well plates using a Chromo 4 continuous fluorescence detector (Bio-Rad). Specific primers for *Ein3* (FP, 5′-AAATGGACCTGCAGCCATAG-3′ and RP, 5-TGAAGCTCCTGCAAAGTGTG-3′) and *ERF1* (FP, 5′-GGCATTACAGAGGTGTTAGACG-3′ and RP, 5′-AAGCAATTG-CAGCTTCTTCA-3′) and the qRT-PCR kit for SYBR Green I (Bio-Rad) were used following the manufacturer's instructions. Reactions (20 μL) contained 10 μL of 2× SYBR Green master mix, 0.5 μM of each primer, and 10 ng of cDNA. Fluorescence threshold data were analyzed using MJ Opticon monitor software version 3.1 (Bio-Rad) and then exported to Microsoft Excel for further analysis. Relative expression levels in each cDNA sample were normalized to the reference gene β-actin.

Metabolite Extraction. Total metabolites were extracted from WT and *Ein3-AS* transgenic tobacco plants at 1 and 48 hpi as previously described.[19] Briefly, the youngest three leaves in plants at 1 and 48 hpi and their corresponding control leaves were collected, immediately frozen in liquid nitrogen, and then stored at −80 °C until metabolite extraction. Frozen samples (200 mg) were ground using a bead beater, suspended in methanol (600 μL) with a 0.125% formic acid solution, kept at 4 °C for 30 min, sonicated at 4 °C for 20 s, and centrifuged at 3000 rpm for 15 min at 4 °C. Finally, the supernatant solution was centrifuged at 13000 rpm for 10 min at 4 °C, and 3 μL of supernatant was then injected into an UPLC-QTOF-MS instrument. Six biological replicates were performed for each experimental condition.

UPLC-QTOF-MS Analysis. Chromatographic separation was performed on an UPLC system (Waters, Milford, MA, USA) using an ACQUITY UPLC BEH C18 column (2.1 mm × 100 mm, 1.7 μm, Waters). The mobile phases consisted of solvent A (0.1% formic acid in deionized water) and solvent B (1% formic acid in acetonitrile). The gradient was applied at a flow rate of 0.4 mL/min as follows: solvent B was linearly increased from 3% at 0 min to 50% at 3 min to 70% at 4 min, increased to 100% at 10 min, and held at 100% until 10.5 min. Finally, solvent B was decreased to 3% at 11 min and held at 3% until 12 min. Mass acquisition was performed on a QTOF-MS (Synapt HDMS system, Waters) operating in both positive (ESI+) and negative (ESI−) electrospray ionization modes with the following parameters: capillary voltage of 3.0 kV for positive and negative modes; cone voltage of 40 V; source temperature of 100 °C; desolvation temperature of 300 °C; and desolvation gas flow of 500 L/h. The mass data were collected in the range of m/z 60−1200 with a scan time of 0.25 s and an interscan time of 0.02 s for 12 min. LC-MS/MS analysis was performed using a collision energy ramp from 20 to 60 eV in the mass range of m/z 60−1200 using automated data-dependent acquisition. To ensure accuracy of the measured mass, leucine-enkephalin (m/z 556.2771 in positive mode and m/z 554.2615 in negative mode) was used as a reference lock-mass compound at a concentration of 500 pg/μL and a flow rate of 5 μL/min.

Data Processing and Statistical Analysis. In total, 48 LC-MS chromatograms in ESI+ mode (48 in ESI− mode) were obtained from WT and *Ein3-AS* transgenic samples collected at two time points after pathogen inoculation (1 and 48 ppi) and their corresponding controls. Detection of mass peaks in the output chromatograms was performed using MarkerLynx software (Waters) with the following parameters: peak intensity threshold of 50 counts and automatic determination of deisotoping, peak width, peak baseline threshold, and noise elimination level. The alignment of mass peaks across all chromatograms was performed using the mass range of m/z 60−1200, mass tolerance of 0.05 Da, retention time window of 0.25 min, and mass window of 0.1 Da. The result was output as a data set containing 2496 and 1055 mass peaks represented as retention time and mass-to-charge ratio (RT−m/z pair) in ESI+ and ESI− modes, respectively.

The intensities of mass peaks for each sample were sum-normalized and Pareto-scaled using the SIMCA-P+ software package. To discriminate between the intensities of mass peaks of the pathogen-inoculated samples and the corresponding controls at each time point, we performed two multivariate statistical analyses, principal component analysis (PCA) and orthogonal partial least squares discriminant analysis (OPLS-DA), with data from 48 samples (8 types of samples × 6 biological replicates). The reliability correlation [p(corr)] values of all metabolites from the S-plot of the OPLS-DA were extracted using the first component. We selected metabolites satisfying the following criteria as potential markers: (a) high confidence ($|p(\mathrm{corr})| > 0.6$) in discrimination between pathogen-inoculated samples and the corresponding controls at each time point; (b) mean intensities in pathogen-inoculated samples significantly different compared to their controls ($p < 0.05$); and (c) fold change of two or more in pathogen-inoculated samples compared to their controls. The p value was calculated using independent two-sample t test. Two-way hierarchical clustering analyses were performed with all of the metabolite mass ions selected as potential *Ppn*-responsive markers, which were differentially regulated during *Ppn* interaction in WT and/or *Ein3-AS* transgenic plants, using PermutMatix (ver. 1.9.3) with Pearson distance and Ward's aggregation method.

Metabolite Identification Based on MS/MS Spectra. For the identification of mass ions selected as potential markers, the following resources were used: (1) the molecular formula assigned by the element composition and isotope composition of precursor ions using MassLynx software; (2) the MS/MS spectra of standard compounds; and (3) metabolome databases including the Human Metabolomics Database (http://www.hmdb.ca/), METLIN (http://metlin.scripps.edu/), LIPD MAPS (http://www.lipidmaps.org/), and Respect for Phytochemicals (http://spectra.psc.riken.jp/). In addition, major fragment ions in the MS/MS spectra of potential markers were compared with literary references on similar compounds. Fragmented or adducted mass features from parent ions were revealed by comparison of their MS/MS spectra.

RESULTS

Impaired Ethylene Signaling Responses in *Ein3-AS* Transgenic Tobacco. At first, we generated independent transgenic tobacco lines constitutively expressing a *35S::Eins3-AS* construct. An antisense *Bam*HI−*Xba*I *Ein3* cDNA fragment (1616 bp) under the constitutive promoter CaMV 35S (Figure 1a) was introduced into tobacco (*N. tabacum* L. cv. Wisconsin 38) using *Agrobacterium*-mediated transformation. We got three independent transgenic lines after monitoring with southern

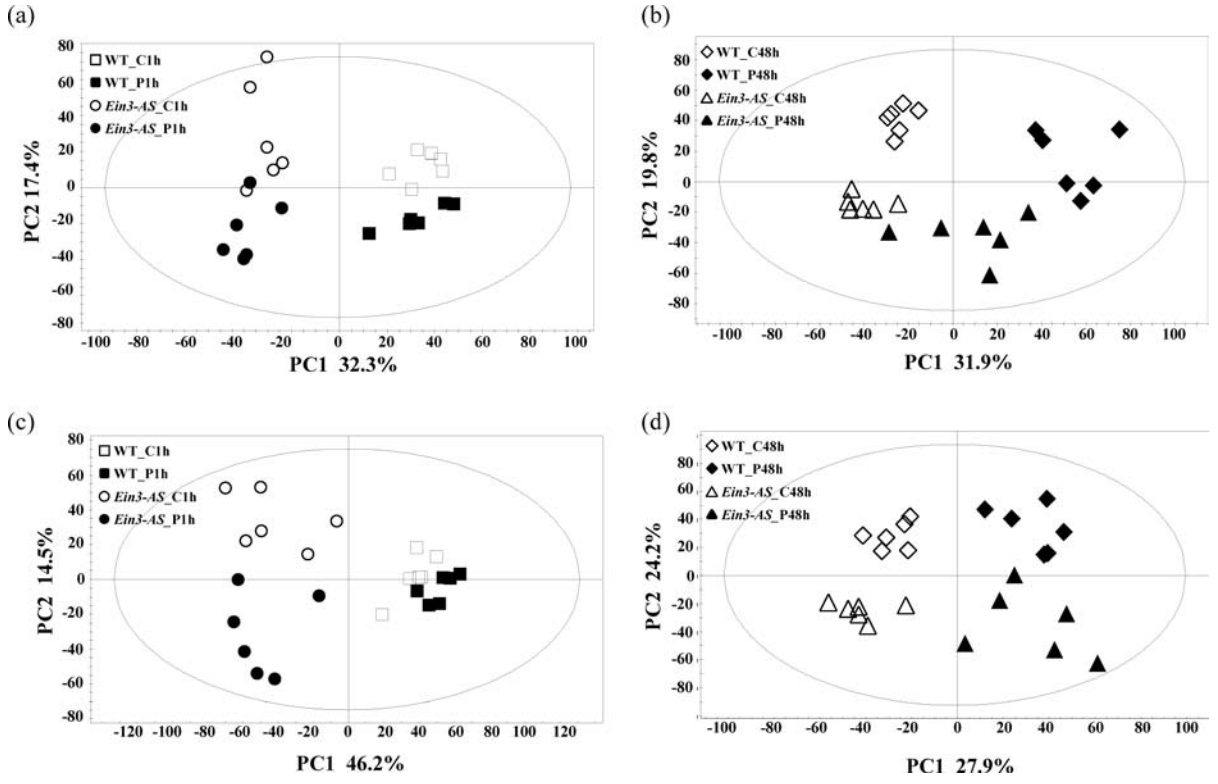

Figure 2. Principal component analysis (PCA) of metabolite ions. PCA of total metabolites at 1 (a, c) and 48 hpi (b, d) extracted from ESI+ (a, b) and ESI− (c, d) modes of UPLC-QTOF-MS. The labels are as follows: WT_P1(48)h and WT_C1(48)h, samples collected at 1 (48) hpi in WT plants and the corresponding control samples, respectively; *Ein3-AS*_P1(48)h and *Ein3-AS*_C1(48)h, samples collected at 1 (48) hpi in *Ein3-AS* transgenic plants and the corresponding control samples. Six biological replicates were performed for each condition (n = 6).

and northern blot analyses. When transgene expression was monitored at the mRNA level by real-time RT-PCR, effective suppression of *Ein3* was detected in all of the transgenic lines, indicating suppression of *Ein3* transcription had constitutively occurred in all three lines (Figure 1b). Redundancy within the *Ein3* family is reported in many plants including tobacco.[20] Five tobacco family members are isolated and then named *NtEIL1* (*N. tabacum Ein3-Like1*) to *NtEIL5*. The sequence identity between the *NtEIL1* cDNA ranges from 48 to 90%, with *NtEIL1/2* and *NtEIL3/4* being highly homologous pairs.[20] Therefore, *Ein3* transcription was not completely blocked in all three transgenic lines, in which we used *NtEIL1* (previously *TEIL1*) for antisense construct of *35S::Eins3-AS*.

EIL1/2 from carnation, which is expressed during development and pollination in the flower, shows a positive correlation with ethylene production.[21] Therefore, we next measured ethylene production in transgenic lines to determine whether or not suppression of *Ein3* expression affects stress-induced ethylene production after treatment with H_2O_2 (Figure 1c). Levels of ethylene production were significantly reduced in three transgenic tobacco lines. In addition to stress-induced ethylene production, basal levels of ethylene production without oxidative stress were also suppressed in all three untreated transgenic lines, indicating *Ein3* transcription was constitutively suppressed.

We chose one transgenic line (#3-1), in which the expression of *Ein3* was strongly suppressed by 36%, compared with WT (Figure 1b), for further experiments. The phenotypic triple-ethylene responses of the seedlings were examined in the presence or absence of ACC, a precursor of ethylene, showing that *Ein3-AS-3* is partially insensitive to ethylene (Figure 1c). Ein3, a transcription factor, has been shown to regulate the transcription of the *ethylene response factor 1* (*ERF1*) gene directly in ethylene signaling. The transcript levels of *Ein3* and *ERF1* were significantly suppressed at 48 hpi (phase II of the ROS burst) after *Ppn* infection in *Ein3-AS* transgenic plants (Figure 1d,e), indicating an effective suppression of pathogen-induced *Ein3* and *ERF1* expression had occurred. However, the suppression of *Ein3* transcription was shown to be less effective at uninfected and 1 hpi after *Ppn* infection in transgenic *Ein3-AS #3-1*, compared to suppression at 48 hpi. Although we did not get any statistical significances ($P < 0.05$) of *Ein3* and *ERF1* suppression in either uninfected control or infected transgenic plants at 1 hpi (Figure 1e,f), the levels of *Ein3* transcription reduced by 30.3 and 25.6% at 0 and 1 hpi, respectively, in the transgenic line. However, these results were statistically significant at $P < 0.1$. Although *ERF1* transcription was suppressed by 81% at 48 hpi, ERF1 transcription was suppressed by 41 and 50%, respectively, at uninfected and 1 hpi after *Ppn* infection as compared with WT plants, which results were also statistically significant at $P < 0.1$ (Figure 1f).

Multivariate Statistical Analysis of Metabolites Profiled in *Ein3-AS* Transgenic Plants after *Ppn* Inoculation. Methanol extracts prepared from leaves collected at 1 and 48 hpi in WT and *Ein3-AS* transgenic plants, and their corresponding control leaves were injected for UPLC-QTOF-MS and output 2469 and 1055 variables (represented by retention time and mass-to-charge ratio (RT−m/z pair)) in ESI + and ESI− modes, respectively. To discriminate among the four sample groups at each time point, the 2469 (1055) variables found in ESI+ (ESI−) mode were subjected to (PCA, showing that four sample groups were clearly separated in the

dx.doi.org/10.1021/jf401785w | J. Agric. Food Chem. 2013, 61, 8477−8489

PC1 × PC2 score plots (Figure 2). Of all of the variables, 32.3% in ESI+ (46.2 in ESI−) mode with the first component at 1 hpi and 19.8% in ESI+ (24.2 in ESI−) mode with the second component at 48 hpi distinguished between WT and *Ein3-AS* transgenic plants. The discrimination between pathogen-inoculated plants and their corresponding controls was detected by 17.4% variables in ESI+ (14.5 in ESI−) mode with the second component at 1 hpi and 31.9% in ESI+ (27.9 in ESI−) mode with the first component at 48 hpi (Figure 2). OPLS-DA score plots showed obvious discrimination between pathogen-inoculated samples and their controls. The selection of *Ppn*-responsive mass ions was performed on the basis of statistical analysis as previously described. In ESI+ mode, 142 and 140 mass ions at 1 hpi and 306 and 123 mass ions at 48 hpi were selected in WT and *Ein3-AS* transgenic plants, respectively. In ESI− mode, 91 and 85 mass ions at 1 hpi and 153 and 86 mass ions at 48 hpi were selected in WT and *Ein3-AS* transgenic plants, respectively. In total, 576 and 336 nonredundant mass ions were selected as potential markers in ESI+ and ESI− modes, respectively (Figure 3); lists are shown in the Supporting Information, Supplementary Table 1.

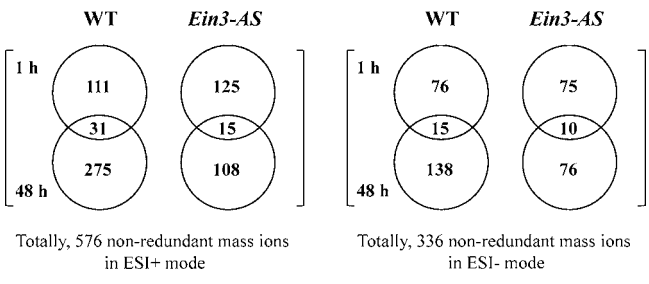

Figure 3. Numbers of metabolite ions selected as potential *Ppn*-responsive markers at 1 and 48 hpi in WT and *Ein3-AS* transgenic plants.

Metabolite Characterization and Identification. To identify the selected mass ions, we performed an integrative analysis of the following information: (1) molecular formulas assigned by element composition analysis and isotope modeling of a precursor ion in MassLynx software; (2) accurate masses (m/z), retention times, and MS/MS spectra of standard compounds; (3) MS and MS/MS spectra analysis using metabolome databases and literary references; and (4) mass differences of identical compounds between ESI+ and ESI− modes. The identification information is presented in Supplementary Table 2 in the Supporting Information. Amino acids such as arginine, serine, threonine, tyrosine, isoleucine/leucine, phenylalanine, and tryptophan were tentatively identified by integrative interpretation of MS-based metabolome database analysis and accuracy of retention time and mass of their standards. Moreover, through MS/MS spectra analysis of the selected mass ions in a metabolome database (http://spectra.psc.riken.jp/), fragmentation patterns of metabolite ions at m/z 132.0801 (0.74_{RT}), 120.0798 (1.34_{RT}), 188.0707 (1.60_{RT}), and 193.0491 (1.75_{RT}) in ESI+ mode were observed to be similar to those of nicotine, phenylalanine $[M + H - CH_2O_2]^+$, tryptophan $[M + H - NH_3]^+$, and scopoletin $[M + H]^+$, respectively. Moreover, an ion at m/z 203.0804 (1.60_{RT}) in ESI− mode was identified as tryptophan $[M - H]^-$ (Supporting Information, Supplementary Table 2).

In ESI+ mode, the MS/MS spectra of mass ions at m/z 470.2283 (1.83_{RT}) and 484.2432 (2.02_{RT}) were observed to be matched to those of dicaffeoyl−spermidine $[M + H]^+$ and caffeoyl-feruloyl−spermidine $[M + H]^+$ detected by HPLC-qTOF-MS in tobacco, respectively.[22] In ESI− mode, a mass ion $[M - H]^-$ at m/z 470.2263 (1.80_{RT}) was shown to be fragmented to m/z 334.1838 (neutral loss of 136.0491 Da; $C_8H_8O_2$, caffeoyl group), 332.1601 (neutral loss of 138.0728 Da; $C_8H_{10}O_2$, dihydrocaffeoyl group), 291.1829 (neutral loss of 179.0500 Da; $C_9H_9NO_3$, dihydroxycinnamamide), and 135.0519 ($C_8H_7O_2^-$, caffeoyl group). Together with the fragment pattern analysis, the molecular ion was identified as caffeoyl-dihydrocaffeoyl−spermidine using MS-based metabolome databases (Supporting Information, Supplementary Figure 1a). Moreover, a metabolite ion $[M - H]^-$ at m/z 482.2281 (2.02_{RT}) was fragmented to m/z 346.1945 (neutral loss of 136.0472 Da; $C_8H_8O_2$, caffeoyl group), 332.1802 (neutral loss of 150.0615 Da; $C_9H_{10}O_2$, feruloyl group), 289.1625 (neutral loss of 193.0792 Da; $C_{10}H_{11}NO_3$, hydroxyl-methoxycinnamide), and 135.0476 ($C_8H_7O_2^-$, caffeoyl group), indicating that the precursor ion is caffeoyl-feruloyl−spermidine (Supporting Information, Supplementary Figure 1b). In addition, through integrative interpretation of molecular formulas ranked from element composition analysis and isotope modeling in MassLynx software and candidates released from accurate mass-based metabolite databases, putrescine $[M + H]^+$ at m/z 89.1073 (1.35_{RT}), feruloyl−putrescine $[M + H]^+$ at 265.1551 (1.60_{RT}) in ESI+ mode and two bis-(dihydrocaffeoyl)−spermidine isomers $[M - H]^-$ at m/z 529.2998 (2.99_{RT}) and 529.3011 (3.37_{RT}) in ESI− mode were tentatively identified, as presented in Supplementary Table 2. We also observed secondary metabolites detected in our previous study,[19] including ferulic acid, tyramine, feruloyl−tyramine, grossamide, hexose-conjugated compounds and a malonylhexose-conjugated compound.

In ESI− mode, galactolipids generate carboxylate anions $[RCOO^-]$ of *sn*-1- and/or *sn*-2-positioned fatty acids and fragment ions derived by neutral loss of fatty acids [RCOOH] or $[RCOOH - H_2O]$. When formic acid is adducted, neutral loss (NL) of 46 Da is generated in their MS/MS spectra. Indeed, molecular ions at m/z 699.3778 (5.14_{RT}) are fragmented to m/z 653.4073 $[M - H - 46]^-$, 415.1451 $[M - H - (16:0 - H_2O)]^-$, 397.1358 $[M - H - (16:0)]^-$, and 255.2223 $[16:0 - H]$, indicating that the molecule is a FA-adducted form and contains palmitic acid (16:0). Furthermore, a metabolite satisfying this requirement was tentatively concluded to be FA-adducted DGMG (16:0) after consideration of the element composition, isotope pattern, and mass accuracy of the precursor ion based on metabolome databases and literary references. According to the analysis procedure, MGMG (16:3) $[M + FA - H]^-$ at m/z 531.2819 (4.48_{RT}), DGMG (16:0) $[M - H]^-$ at m/z 653.3739 (5.15_{RT}), MGDG (16:0/18:3) $[M + FA - H]^-$ at m/z 797.5352 (9.36_{RT}), MGDG (16:3/17:3) $[M + FA - H]^-$ at m/z 777.4781 (9.52_{RT}), DGDG (16:2/18:3) $[M + FA - H]^-$ at m/z 955.5599 (9.76_{RT}), MGDG (16:1/18:3) $[M + FA - H]^-$ at m/z 767.4920 (10.39_{RT}), and MGDG (16:2/18:3) $[M + FA - H]^-$ at m/z 793.4987 (10.46_{RT}) were identified (Supporting Information, Supplementary Table 2). In addition, in the case of glycerophospholipids in ESI− mode, their MS/MS spectra generate specific daughter ions, including carboxylate anion $[RCOO^-]$ of *sn*-1- and/or *sn*-2-positioned fatty acids, fragment ions derived from neutral loss of fatty acids [RCOOH] or

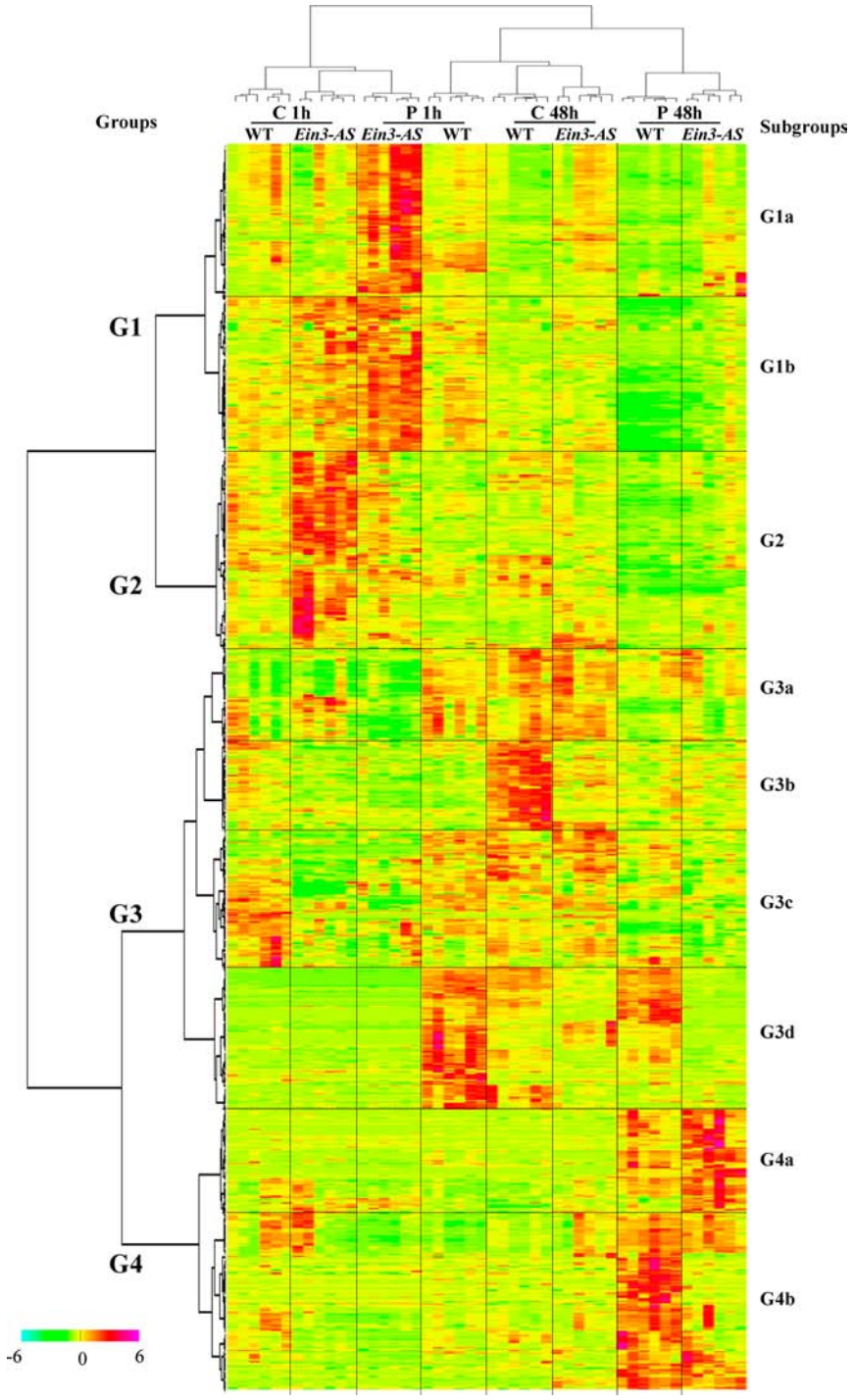

Figure 4. Two-way hierarchical clustering analysis. A heat map was generated with all of the metabolite mass ions that were differentially regulated during *Ppn* interaction in WT and/or *Ein3-AS* transgenic plants. Each colored cell represents the normalized intensity of each mass ion according to the color scale. Rows: total 912 metabolite ions (576 positive and 336 negative ions). Columns: *Ppn*-inoculated WT and *Ein3-AS* plants and their corresponding controls (6 biological replicates × 8 conditions, n = 48).

$[RCOOH - H_2O]$, m/z 171 $[GP - H]^-$, 153 $[GP - H_2O - H]^-$, and 79 $[PO_3]^-$. A molecular ion at m/z 452.2790 (5.36_{RT}) was shown to be fragmented to 255.2279 $[16{:}0 - H]^-$ and 78.9585 $[PO_3]^-$, indicating that the molecule is a glycerophospholipid with palmitic acid (16:0). Together with these results, accurate mass-based metabolite analysis in metabolome databases revealed that the molecular ion is lysoPE (16:0). In ESI+ mode, one (m/z 86 $[C_5H_{12}N]^+$) specific daughter ion of phosphatidylcholine (PC) and lysoPC was observed in MS/MS spectra of molecular ions at m/z 769.4849 (9.97_{RT}), 783.5003 (10.20_{RT}), and 766.5428 (10.44_{RT}), indicating that the molecules were PCs or lysoPCs (Supporting Information, Supplementary Table 2).

Furthermore, on the basis of the molecular formulas assigned by isotope pattern analysis of a precursor ion using MassLynx, literary reference, and accurate mass-based metabolome database analysis, sphingosine $[M + H]^+$ at m/z 300.2939 (4.27_{RT}), phytosphingosine $[M + H]^+$ at m/z 318.3015

Table 1. Means of Normalized Signal Intensities of Identified Mass Ions as Potential Markers in *Ppn*-Inoculated WT and *Ein3-AS* Transgenic Plants

				average intensity in WT						average intensity in *Ein3-AS*					
RT_mass (min_m/z)	adduct form	tentative identification	group[a]	C_{1h}[b,c]	P_{1h}[b,c]	p[d]	C_{48h}	P_{48h}	p[b,c]	C_{1h}	P_{1h}	p[b,c]	C_{48h}	P_{48h}	p[b,c]
4.48_531.2819	$[M + FA - H]^-$	MGMG (16:3)	G1a	7.2	9.5	0.2058	4.4	7.0	0.4701	12.5	28.6	0.0368	7.4	19.1	0.1360
5.14_699.3778	$[M + FA - H]^-$	DGMG (16:0)	G1a	3.9	5.6	0.1049	4.9	4.0	0.5202	4.0	26.4	0.0006	5.4	6.9	0.6631
5.15_653.3739	$[M - H]^-$	DGMG (16:0)	G1a	2.9	4.3	0.2732	4.3	3.1	0.3793	2.9	24.6	0.0010	5.2	7.1	0.4938
6.74_277.2181	$[M - H]^-$	octadecatrienoic acid	G1a	1.3	1.9	0.1188	0.9	1.9	0.0939	2.4	4.9	0.0159	1.5	3.7	0.0709
9.52_777.4781	$[M + FA - H]^-$	MGDG (16:3/17:3)	G1b	10.5	8.1	0.1183	5.7	2.3	0.0006	13.2	21.6	0.0094	6.0	6.1	0.9533
9.76_955.5599	$[M + FA - H]^-$	DGDG (16:2/18:3)	G1b	38.0	24.8	0.0325	22.6	11.1	0.0016	46.9	72.6	0.0107	20.4	30.4	0.0500
9.97_769.4849	$[M + H]^+$	PC class compound	G1b	137.9	145.8	0.6483	109.5	54.0	0.0104	188.5	231.5	0.1586	177.4	106.3	0.0059
10.20_783.5003	$[M + H]^+$	PC class compound	G1b	42.2	38.3	0.3878	31.1	14.9	0.0022	52.2	50.0	0.6671	31.3	22.1	0.0692
10.39_767.4920	$[M + FA - H]^-$	MGDG (16:1/16:3)	G1b	29.4	29.1	0.9442	23.8	11.5	0.0009	35.0	48.5	0.1106	20.3	18.9	0.7678
10.44_766.5428	$[M + H]^+$	PC (35:5)	G1b	56.2	51.1	0.4809	40.2	17.1	0.0002	74.8	80.6	0.2907	41.6	34.2	0.0953
10.46_793.4987	$[M + FA - H]^-$	MGDG (16:2/18:3)	G1b	100.6	103.7	0.9399	81.8	28.3	0.0393	137.4	178.8	0.4362	95.7	75.3	0.4452
0.62_104.0366	$[M - H]^-$	serine	G2	6.8	2.3	0.0000	3.7	3.4	0.4104	9.3	5.8	0.0058	4.4	5.2	0.5032
0.62_118.0517	$[M - H]^-$	threonine	G2	6.1	5.2	0.3705	11.3	5.3	0.0064	10.5	3.5	0.0001	6.0	4.5	0.1242
1.34_120.0798	$[M + H - CH_2O_2]^+$	phenylalanine	G2	80.9	35.9	0.0015	33.6	44.5	0.0946	144.7	66.1	0.1109	66.7	65.1	0.9373
1.34_164.0719	$[M - H]^-$	phenylalanine	G2	33.7	13.2	0.0006	15.5	15.9	0.9156	57.7	36.6	0.1959	32.7	24.0	0.2761
1.34_166.0875	$[M + H]^+$	phenylalanine	G2	11.6	5.4	0.0123	4.9	8.3	0.0724	18.5	12.4	0.2757	12.1	9.7	0.5508
5.39_297.2451	$[M - H]^-$	hydroxyoctadecenoic acid	G2	6.4	4.7	0.3893	5.2	3.0	0.0120	5.3	7.7	0.3252	5.4	2.3	0.0482
9.36_797.5352	$[M + FA - H]^-$	MGDG (16:0/18:3)	G2	50.3	43.7	0.7497	49.7	18.6	0.0009	59.3	54.8	0.8570	38.7	38.6	0.9941
0.59_173.1040	$[M - H]^-$	arginine	G3a	13.4	44.0	0.0001	58.2	48.0	0.3047	14.7	12.1	0.7037	55.7	43.0	0.2923
2.99_529.2998	$[M - H]^-$	bis(dihydrocaffeoyl)−spermine (1)	G3a	42.2	60.0	0.1988	42.1	12.0	0.0127	81.8	24.3	0.0070	50.1	23.8	0.0020
3.37_529.3011	$[M - H]^-$	bis(dihydrocaffeoyl)−spermine (2)	G3a	11.8	17.0	0.3397	12.6	4.4	0.0274	24.5	8.5	0.0434	19.9	9.9	0.0027
0.74_132.0801	+	nicotine	G3c	72.6	77.9	0.3567	122.0	74.0	0.0347	25.2	56.2	0.0000	62.9	48.1	0.2215
1.20_151.0745	$[M + H]^+$	hydrocinnamic acid	G4a	2.5	0.7	0.3383	2.0	25.9	0.0682	1.0	1.9	0.0351	0.9	48.9	0.0014
1.75_193.0491	$[M + H]^+$	scopoletin	G4a	6.2	0.5	0.3153	7.8	16.6	0.3029	4.1	1.2	0.1697	0.8	80.3	0.0047
2.83_805.3267	$[M + H]^+$	hexose conjugate	G4a	16.2	7.9	0.0620	10.3	35.7	0.0002	20.6	11.6	0.2361	16.4	58.3	0.0000
2.84_314.1369	$[M + H]^+$	feruloyltyramine	G4a	0.4	0.5	0.2161	0.5	15.2	0.0052	0.6	1.0	0.1613	0.5	44.3	0.0030
2.85_312.1220	$[M - H]^-$	feruloyl−tyramine	G4a	0.6	0.7	0.1012	0.5	33.0	0.0118	1.3	2.4	0.1213	1.0	101.3	0.0028
3.21_803.3112	$[M - H]^-$	hexose conjugate	G4a	19.4	5.6	0.0243	10.2	25.1	0.0004	8.4	5.9	0.4724	13.6	30.2	0.0074
3.21_805.3299	$[M + H]^+$	hexose conjugate	G4a	8.7	3.7	0.0429	6.2	15.6	0.0005	5.8	2.7	0.1908	9.1	17.5	0.0369
3.50_623.2345	$[M - H]^-$	grossamide	G4a	0.7	0.5	0.4089	0.5	15.8	0.0013	1.1	1.0	0.8774	0.7	58.2	0.0061
4.27_300.2939	$[M + H]^+$	sphingosine	G4a	1.4	1.6	0.3188	1.3	1.7	0.2576	1.7	2.5	0.0154	1.6	3.3	0.0011
4.28_318.3015	$[M + H]^+$	phytosphingosine	G4a	10.3	12.0	0.0541	9.4	12.6	0.0700	13.2	18.8	0.0002	11.8	25.6	0.0022
5.04_291.1983	$[M - H]^-$	keto-octadecatrienoic acid isomer (1)	G4a	0.5	0.6	0.1867	0.5	2.6	0.0501	2.4	1.7	0.3301	1.3	10.5	0.0280
5.17_295.2289	$[M - H]^-$	hydroxyoctadecadienoic acid	G4a	1.5	0.7	0.0320	1.0	2.7	0.1157	3.6	2.5	0.2806	2.4	10.0	0.0199
5.35_454.2965	$[M + H]^+$	lysoPE (16:0)	G4a	2.1	2.0	0.8192	0.6	2.1	0.0218	3.1	3.1	0.8708	2.5	4.3	0.0941
5.36_452.2790	$[M - H]^-$	lysoPE (16:0)	G4a	8.2	7.7	0.6921	3.4	8.8	0.0270	16.0	17.5	0.4993	10.0	19.8	0.0786
5.37_496.3413	$[M + H]^+$	lysoPC (16:0)	G4a	11.4	12.0	0.6452	5.4	11.2	0.0266	18.2	14.5	0.1287	13.3	17.6	0.1498
5.98_291.1977	$[M - H]^-$	keto-octadecatrienoic acid isomer (2)	G4a	0.4	0.4	0.5550	0.4	2.4	0.0868	0.3	0.5	0.0254	0.4	10.4	0.0402
1.00_180.0674	$[M - H]^-$	tyrosine	G4b	12.3	2.8	0.0132	4.7	11.3	0.0099	12.9	3.2	0.0780	12.7	10.5	0.5636
1.14_132.0984	$[M + H]^+$	isoleucine/leucine	G4b	2.4	3.4	0.4879	2.3	9.8	0.0209	2.9	0.5	0.0142	8.5	0.7	0.0132
1.15_130.0853	$[M - H]^-$	isoleucine/leucine	G4b	5.3	9.4	0.0778	6.6	15.4	0.0126	7.1	4.4	0.2162	15.1	3.9	0.0197
1.35_89.1073	$[M + H]^+$	putrescine	G4b	5.4	3.1	0.1118	3.4	12.1	0.0457	1.8	0.6	0.1060	2.0	6.2	0.0753

dx.doi.org/10.1021/jf401785w | J. Agric. Food Chem. 2013, 61, 8477−8489

Table 1. continued

RT_mass (min_m/z)	adduct form	tentative identification	group[a]	average intensity in WT						average intensity in *Ein3-AS*					
				C_{1h}[b,c]	P_{1h}[b,c]	p[d]	C_{48h}	P_{48h}	p[b,c]	C_{1h}	P_{1h}	p[b,c]	C_{48h}	P_{48h}	p[b,c]
1.59_146.0604	+	tryptophan	G4b	89.8	27.9	0.0168	51.3	139.0	0.0001	63.2	23.9	0.1092	60.5	111.4	0.0207
1.59_159.0931	$[M - H]^-$	tryptamine	G4b	12.3	4.1	0.0124	7.9	14.4	0.0001	11.6	5.3	0.1192	9.9	14.9	0.0687
1.60_177.0549	$[M + H - H_2O]^+$	ferulic acid	G4b	16.8	7.2	0.0987	8.7	25.4	0.0180	9.0	3.1	0.0400	10.2	34.9	0.0363
1.60_188.0707	$[M + H - NH_3]^+$	tryptophan	G4b	144.0	45.1	0.0233	78.7	225.8	0.0001	99.9	40.6	0.1324	104.1	184.4	0.0435
1.60_203.0804	$[M - H]^-$	tryptophan	G4b	142.8	41.2	0.0112	81.6	172.0	0.0000	127.1	58.2	0.1480	111.4	163.6	0.1018
1.60_265.1551	$[M + H]^+$	feruloylputerscine	G4b	16.5	7.0	0.1066	7.3	22.1	0.0161	9.5	3.7	0.0086	9.8	31.4	0.0443
1.80_470.2263	$[M - H]^-$	caffeoyl-dihydrocaffeoyl−spermidine	G4b	78.1	32.0	0.0212	106.1	156.5	0.3595	15.7	0.8	0.1097	10.0	18.8	0.4815
1.83_470.2283	$[M + H]^+$	dicaffeoyl−spermidine	G4b	82.5	65.6	0.5632	115.3	380.6	0.0273	16.2	1.5	0.0355	39.1	93.9	0.1565
2.02_482.2281	$[M - H]^-$	caffeoyl-feruloyl−spermidine	G4b	19.6	11.1	0.0795	22.3	50.5	0.0215	2.4	0.7	0.1237	8.2	17.8	0.2922
2.02_484.2432	$[M + H]^+$	caffeoyl-feruloyl−spermidine	G4b	42.0	36.1	0.5529	48.7	86.5	0.0348	7.4	1.1	0.0237	24.4	38.9	0.3171
2.98_805.3219	$[M - H]^-$	hexose conjugate	G4b	272.6	137.8	0.0064	110.4	268.9	0.0001	71.8	47.9	0.4809	158.9	204.0	0.5615
2.98_807.3451	$[M + H]^+$	hexose conjugate	G4b	135.9	87.2	0.1067	64.5	259.3	0.0000	35.8	20.0	0.2822	94.2	133.3	0.5078
3.08_891.3202	$[M - H]^-$	malnoylhexose conjugate	G4b	68.7	24.1	0.0903	19.6	133.1	0.0001	10.4	5.9	0.4458	42.6	52.3	0.7858
3.08_893.3452	$[M + H]^+$	malnoylhexose conjugate	G4b	48.9	21.5	0.1497	18.8	119.8	0.0004	8.1	3.7	0.2492	38.8	43.2	0.8904

[a]The identified mass ions are grouped on the basis of two-way hierarchical clustering analysis. [b,c]Mean of the normalized signal intensities of each mass ion at 1 and 48 h control (C_{1h} and C_{48h}) and 1 and 48 h post pathogen inoculation (P_{1h} and P_{48h}) in WT and *Ein3-AS* transgenic plants. [d]p value is calculated using independent two-sample t test between pathogen-inoculated samples and their corresponding controls at each time point.

dx.doi.org/10.1021/jf401785w | J. Agric. Food Chem. 2013, 61, 8477−8489

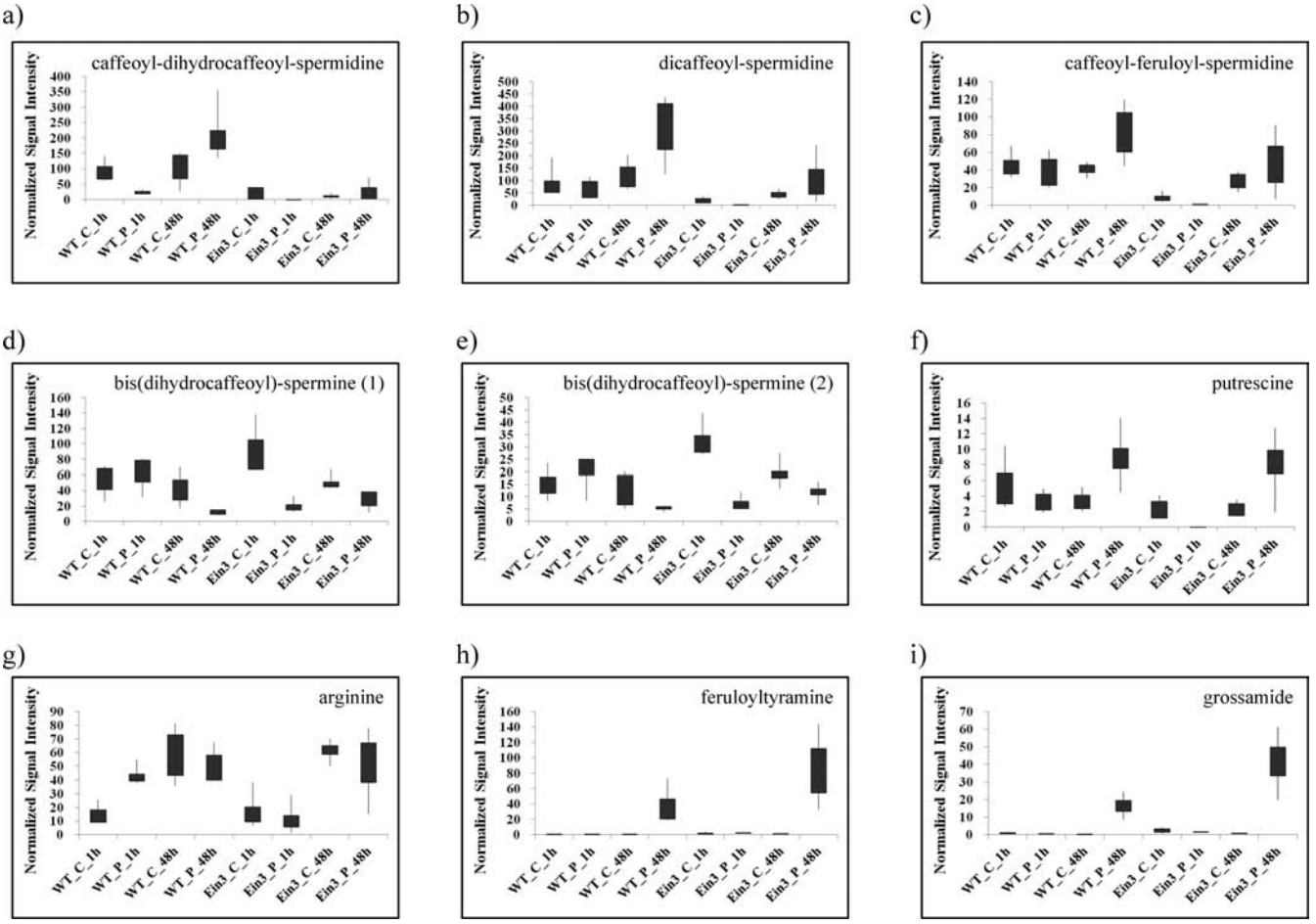

Figure 5. Box-and-whisker plots for accumulation changes of polyamine conjugates and their intermediates in *Ppn*-inoculated WT and *Ein3-AS* transgenic plants: (a) caffeoyl-dihydrocaffeoyl−spermidine $[M - H]^-$; (b) dicaffeoyl−spermidine $[M + H]^+$; (c) caffeoyl-feruloyl−spermidine $[M + H]^+$; (d) bis(dihydrocaffeoyl)−spermine (1) $[M - H]^-$; (e) bis(dihydrocaffeoyl)−spermine (2) $[M - H]^-$; (f) putrescine $[M + H]^-$; (g) arginine $[M - H]^-$; (h) feruloyltyramine $[M - H]^-$; (i) grossamide $[M - H]^-$. Maximum and minimum values of a metabolite among six biological replicates are represented at upper and lower ends of whisker, respectively, and their 75th and 25th percentiles are represented at upper and lower ends of box, respectively.

(4.28_{RT}), lysoPE (16:0) $[M + H]^+$ at m/z 454.2965 (5.35_{RT}), lysoPC (16:0) $[M + H]^+$ at m/z 496.3413 (5.37_{RT}), and PC (38:7) $[M + H]^+$ at m/z 804.5532 (8.92_{RT}) and in ESI− mode keto-octadecatrienoic acid $[M - H]^-$ at m/z 291.1983 (5.04_{RT}), hydroxyoctadecadienoic acid $[M - H]^-$ at m/z 295.2289 (5.17_{RT}), hydroxyoctadecenoic acid $[M - H]^-$ at m/z 297.2451 (5.39_{RT}), keto-octadecatrienoic acid $[M - H]^-$ at m/z 291.1977 (5.98_{RT}), and octadecatrienoic acid $[M - H]^-$ at m/z 277.2181 (6.74_{RT}) were identified.

Two-Way Hierarchical Clustering Analysis. To compare accumulation patterns of *Ppn*-induced mass ions in WT and *Ein3-AS* transgenic plants, we performed two-way hierarchical clustering analysis using Pearson correlation as a distance metric. The analysis showed that *Ppn*-inoculated samples are divided into three groups, and the mass ions selected as potential markers are divided into four main groups (Figure 4). The clustering analysis of the *Ppn*-inoculated samples revealed the following three groups: WT and *Ein3-AS* at 1 h control and *Ein3-AS* at 1 hpi; WT and *Ein3-AS* at 48 h control and WT at 1 hpi; and WT and *Ein3-AS* at 48 hpi. This result indicates that the majority of the selected mass ions differ between WT and *Ein3-AS* at 1 hpi.

The normalized signal intensities of the G1-grouped mass ions were highest at 1 hpi in *Ein3-AS* transgenic plants (Figure 4). G1a, one subgroup of G1, includes mass ions MGMG (16:3), DGMG (16:0), and octadecatrienoic acid (18:3) (Table 1), which are strongly increased at 1 hpi in *Ein3-AS* transgenic plants compared to the corresponding control plants. The other subgroup (G1b) includes mass ions increased at 1 hpi in *Ein3-AS* transgenic plants and decreased at 48 hpi in WT plants, containing MGDG (16:1/16:3), MGDG (16:2/18:3), MGDG (16:3/17:3), DGDG (16:2/18:3), and three PCs (Table 1). G2, whose most mass ions showed the strongest expression in *Ein3-AS* transgenic plant at control 1 h (Figure 4), includes serine, threonine, phenylalanine, hydroxyocatadecenoic acid, and MGDG (16:0/18:3) (Table 1 and Supplementary Figure 2 in the Supporting Information). The mass ions in G3 showed complicated accumulation patterns at each time point and were divided into four subgroups (G3a−G3d). Mass ions grouped in G3a (Figure 4), including two bis(dihydrocaffeoyl)−spermine isomers (Table 1), seemed to be increased and decreased at 1 and 48 hpi, respectively, in WT but decreased at 1 and 48 hpi in *Ein3-AS* transgenic plants compared to their corresponding controls. The G3b-grouped mass ions showed the highest signal intensities in WT plants at control 48 h. The majority of the G3c-grouped mass ions, including nicotine (Table 1), showed lower signal intensities at 1 h in untreated *Ein3-AS* transgenic plants compared to WT plants. G3d mass ions

dx.doi.org/10.1021/jf401785w | J. Agric. Food Chem. 2013, 61, 8477−8489

showed a strong increase at 1 h after *Ppn* inoculation in WT plants. We failed to identify any of the mass ions in this group. In addition, the normalized signal intensities of mass ions in G4 were strongly increased at 48 hpi in WT and *Ein3-AS* transgenic plants (Figure 4). Hydrocinnamic acid, scopoletin, two hexose conjugates, feruloyltyramine, grossamide, sphingosine, phytosphingosine, two keto-octadecatrienoic acid isomers, hydroxyoctadecadienoic acid lysoPE (16:0), and lysoPC (16:0) were grouped into G4a (Table 1). Their increased signal intensities at 48 hpi were higher in *Ein3-AS* transgenic plants than in WT plants. The majority of mass ions in G4b showed the highest signal intensities at 48 hpi in WT plants; these species included tyrosine, isoleucine/leucine, tryptophan, tryptamine, putrescine, ferulic acid, feruloyl−puterscine, caffeoyl-dihydrocaffeoyl−spermidine, dicaffeoyl−spermidine, caffeoyl-feruloyl−spermidine, one hexose conjugate, and one malnoylhexose conjugate (Table 1).

DISCUSSION

Previously, our research group reported a biphasic ROS burst after inoculation of a WT tobacco cultivar, *N. tabacum* L. cv. Wisconsin 38, with a hemibiotrophic fungal pathogen, *P. parasitica* var. *nicotianae* (*Ppn*).[3] Unlike the ROS burst that occurs during incompatible interactions accompanied by enhanced resistance to biotrophic pathogens, the ROS burst caused by interaction between *Ppn* and this susceptible tobacco induced necrotic cell death. Interestingly, ethylene production also showed a biphasic pattern after *Ppn* inoculation. The production of ethylene and ROS is significantly reduced in ROS or ethylene biosynthesis/signaling-impaired transgenic plants, which alleviates necrotic cell death caused by *Ppn*.[3] This result indicates a link between ethylene and ROS accumulation in *Ppn*-induced necrotic cell death. We reported metabolic changes, occurring at each phase of the ROS burst, that may be related to defense and/or susceptibility responses to *Ppn*.[19] However, how the biphasic production of ROS and ethylene mediates plant defense responses to *Ppn* is still unknown. To obtain more detailed information, we focused on metabolic changes related to the ROS and ethylene burst after *Ppn* inoculation. For this analysis, we performed metabolic profiling in ethylene signaling-impaired transgenic plants, *Ein3-AS*, which showed a more tolerant phenotype to *Ppn* than WT plants.[3] The phenotypic ethylene triple response of these seedlings and suppression of *Ein3* and *ERF1* transcripts (Figure 1) showed that the Ein3-mediated pathway is impaired in *Ein3-AS* transgenic plants, causing partial insensitivity to ethylene.

We performed nontargeted total metabolite profiling at 1 (first phase of ROS burst) and 48 h (second phase) after *Ppn* inoculation in WT and *Ein3-AS* transgenic tobacco plants using UPLC-QTOF-MS.[19] UPLC-QTOF-MS analysis of methanol extracts at 1 and 48 hpi in WT and *Ein3-AS* transgenic plants separated several thousand mass ions. The output mass ions were subjected to statistical analysis to select *Ppn*-responsive mass ions, revealing 576 and 336 nonredundant mass ions in ESI+ and ESI− modes, respectively (Figure 3). Through integrative interpretation of information from (1) molecular formulas assigned by isotope pattern analysis of a precursor ion using MassLynx software, (2) analysis of standards such as amino acids, and (3) accurate MS and MS/MS spectra analysis using metabolome databases and literary references, a total of 56 mass ions were identified (Supporting Information, Supplementary Table 2).

The majority of the identified mass ions were related to hydroxycinnamic acid amides (HCAAs), which are involved in a wide range of fundamental processes in plants, including cell division, flowering, membrane stabilization, and defense responses to abiotic and biotic stresses.[23] Hierarchical clustering analysis showed that HCAAs are differentially accumulated after *Ppn* inoculation of WT and *Ein3-AS* transgenic plants. Three polyamine-derived HCAAs (caffeoyl-dihydrocaffeoyl−spermidine, dicaffeoyl−spermidine, and caffeoyl-feruloyl−spermidine) (Figure 5a−c) showed strong reductions in their basal and *Ppn*-stimulated levels in *Ein3-AS* transgenic plants, in which the resistance to *Ppn* is enhanced and the second burst of ROS and ethylene is abrogated,[3] compared to WT plants. The levels of two bis-(dihydrocaffeoyl)−spermine isomers (Figure 5d,e) were shown to be significantly reduced at 1 hpi in *Ein3-AS* transgenic plants, but not in WT. The biosynthesis of polyamines (putrecine, spermidine, and spermine) in plants is initiated by decarboxylation of arginine or ornithine to putrecine.[23] During HR to tobacco mosaic virus (TMV) infection and incompatible plant−pathogen (herbivore) interactions, the accumulation of free polyamines and polyamine conjugates and the activation of arginine decarboxylase (ADC) and ornithine decarboxylase (ODC) are increased in tobacco and pepper plants.[24−28] The HR-specific expression of *ODC1* in pepper has been reported to be regulated in an SA-independent and JA- and/or ET-dependent manner.[24] Furthermore, enzymes involved in the conjugation of hydroxycinnamic acid and polyamines are reported to be controlled by the JA-dependent transcription factor NaMYB8 in the tobacco *N. attenuate*.[28,29] Together with the results, the reduction of the basal and *Ppn*-induced levels of the polyamine-derived HCAAs, putrecine, and arginine in *Ein3-AS* transgenic plants (Figure 5a−g) proposes that the production of the compounds is most likely ethylene signaling (Ein3) dependent.

In addition, the tyramine-derived HCAAs such as feruloyl−tyramine (FT) and grossimide grouped into G4a were identified as potential markers of *Ppn* infection. FT and grossimide contribute to plant defense against pathogens via their peroxidative incorporation into the cell wall to form covalent cross-linked polymers and their antibiotic activity.[30,31] Accumulation of FT and activation of tyramine hydroxycinnamoyltransferase (THT), which catalyzes the conjugation of ferulic acid and tyramine, were observed in wounded leaf segments of maize,[32] HR-stimulated pepper,[33] and scab lesion-wounded potato.[34] In this study, FT and grossimide were dramatically increased in both WT and *Ein3-AS* transgenic plants at 48 hpi (the second burst of ROS) (Figure 5h,i). The increased levels were significantly higher in *Ein3-AS* transgenic plants compared to WT. The basal and *Ppn*-induced levels of ferulic acid and tyrosine, a substrate for tyramine biosynthesis, were similar in WT and *Ein3-AS* transgenic plants during *Ppn* interaction. The results indicate that there is an ethylene signaling (Ein3)-independent pathway for the accumulation of tyramine-derived HCAAs during *Ppn* interaction in *N. tabacum* L. cv. Wisconsin 38. Indeed, FT and THT activation has been reported to be increased in pepper during HR-induced incompatible interaction.[35] However, pretreatment with lipopolysaccharide, a ubiquitous component of Gram-negative bacteria, induced suppression of HR derived from incompatible interaction, enhanced proliferation of incompatible pathogens, and accelerated FT synthesis and THT activation, suggesting

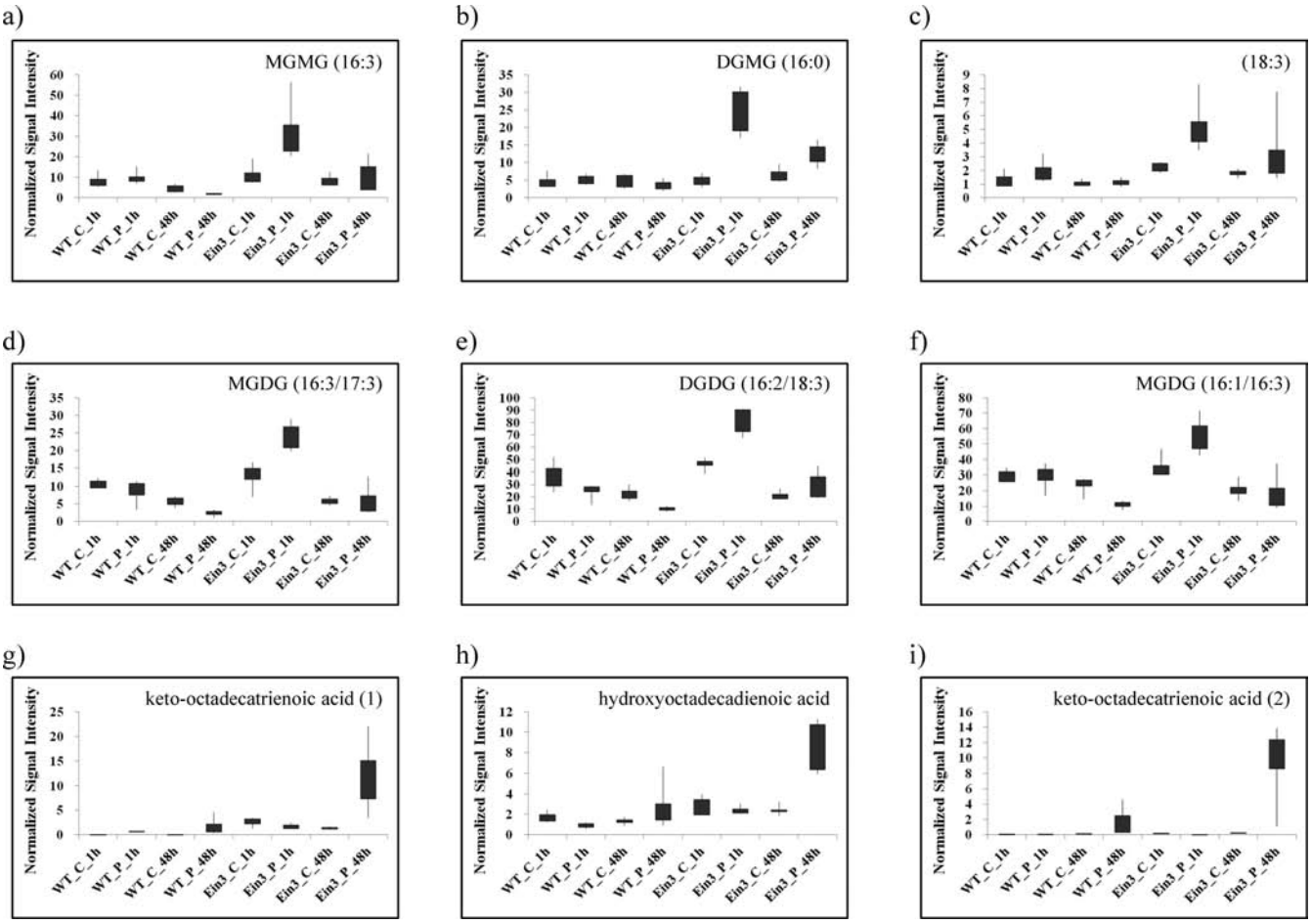

Figure 6. Box-and-whisker plots for accumulation changes of galactolipids and oxidized fatty acids in *Ppn*-inoculated WT and *Ein-AS* transgenic plants: (a) MGMG (16:3) $[M + FA - H]^-$; (b) DGMG (16:0) $[M + FA - H]^-$; (c) octadecatrienoic acid (18:3) $[M - H]^-$; (d) MGDG (16:3/17:3) $[M + FA - H]^-$; (e) DGDG (16:2/18:3) $[M + FA - H]^-$; (f) MGDG (16:1/16:3) $[M + FA - H]^-$; (g) keto-octadecatrienoic acid (1) $[M - H]^-$; (h) hydroxyoctadecadienoic acid $[M - H]^-$; (i) keto-octadecatrienoic acid (2) $[M - H]^-$.

that FT synthesis is independent of HR linked with ethylene signaling.[33,35]

The quantitative *Ppn*-induced changes of galactolipids, which are the major lipids present in the plastid membrane in plants, were observed to differ between *Ein3-AS* transgenic plants and WT (Figure 6). MGMG (16:3) and DGMG (16:0), which are produced by hydrolysis of a fatty acid at the *sn*-1 or -2 position of diacylglycerol lipids, and octadecatrienoic acid (18:3), a major substrate of oxylipins, showed dramatic increases at 1 hpi in *Ein3-AS* transgenic plants (Figure 6a–c). Furthermore, galactosyl-diacylglycerol lipids such as MGDG (16:3/17:3), DGDG (16:2/18:3), and MGDG (16:1/16:3) also showed to be strongly increased at 1 hpi in *Ein3-AS* transgenic plants. However, they were significantly decreased at 48 hpi in WT but not changed in *Ein3-AS* transgenic plants (figure 6d–f). The compositional changes of galactolipids in WT and *Ein3-AS* transgenic plants may reflect metabolic rearrangements occurring in plastid membrane to acclimate or overcome cell damage derived from *Ppn* attack.

Levels of oxidized free fatty acids such as two keto-octadecatrienoic acid isomers and hydroxyoctadecadienoic acid were strongly increased in *Ein3-AS* transgenic plants at 48 hpi but weakly increased in WT (Figure 6g–i). Oxidation of membrane lipids in plants is believed to mediate defense responses to stresses and to prevent oxidative damage.[36,37] In particular, trienoic fatty acids have been suggested to act as ROS sinks, reducing ROS levels and protecting against adverse ROS effects during fungal infection and chronic oxidative stress responses.[38,39] The oxidized products of unsaturated fatty acids, oxylipins, act as signaling molecules that activate defense systems against wounding and pathogen attack.[38,40] The hemibiotrophic oomycete pathogen *Phytophthora infestans*[41] and fungal elicitors such as cryptogein[42] activate the HR-linked 9-lipoxygenase pathway, which leads to peroxidation at the C-9 position of octadecatrienoic acid (18:3) and octadecadienoic acid (18:2). HR is initiated by recognition of the Avr protein by a host R protein (incompatible interaction). On the other hand, in the absence of an R protein in the host, the Avr protein promotes virulence in plant (compatible interaction). The expression of AvirRpm1, a bacterial avirulence protein, in planta (incompatible interaction) induces dramatic accumulation of oxylipins, such as keto-octadecadi(tri)enoic acid, hydro(pero)-xyoctadecadi(tri)enoic acid, 12-oxophytodienoic acid, jasmonic acid, and their substrates, such as octadecatrienoic acid (18:3) and octadecadienoic acid (18:2). However, during compatible interaction, there is little to no accumulation of these species.[43] The results suggest that the accumulation of the oxidized fatty acids in *Ein3-AS* transgenic plants are most likely involved in defense response to *Ppn* and may be negatively associated with an ethylene signaling pathway.

dx.doi.org/10.1021/jf401785w | J. Agric. Food Chem. 2013, 61, 8477–8489

■ ASSOCIATED CONTENT

Supporting Information

Supplementary Figure 1: Analysis of MS/MS fragmentation of caffeoyl-dihydrocaffeoyl-spermidine at *m/z* 470.2268 (a) and caffeoyl-feruloyl−spermidine at *m/z* 482.2281 (b) in ESI− mode. NL represents neutral loss. Supplementary Figure 2: Box-and-whisker plots for accumulation changes of identified mass ions as potential markers in *Ppn*-inoculated WT and *Ein3-AS* transgenic plants. Supplementary Table 1a: Means of sum-normalized signal intensities of 576 nonredundant mass ions detected as potential markers in positive mode. Supplementary Table 1b: Means of sum-normalized signal intensities of 336 nonredundant mass ions detected as potential markers in negative mode. Supplementary Table 2: Identification of *Ppn*-induced mass ions in WT and *Ein3-AS* transgenic tobacco plants. This material is available free of charge via the Internet at http://pubs.acs.org.

■ AUTHOR INFORMATION

Corresponding Author

*(M.H.N.) Phone: 82-2-6943-4132. Fax: 82-2-6943-4109. E-mail: nammh@kbsi.re.kr.

Funding

This work was supported by a grant from KBSI (T32602) to M.H.N. and a grant from the National Research Foundation of Korea (Grant 2012-000-4329) to K.Y.P.

Notes

The authors declare no competing financial interest.

■ ACKNOWLEDGMENTS

We gratefully acknowledge Seong Hwa Park for technical support.

■ REFERENCES

(1) Torres, M. A.; Jones, J. D.; Dangl, J. L. Reactive oxygen species signaling in response to pathogens. *Plant Physiol.* **2006**, *141*, 373−378.

(2) Torres, M. A.; Dangl, J. L. Functions of the respiratory burst oxidase in biotic interactions, abiotic stress and development. *Curr. Opin. Plant Biol.* **2005**, *8*, 397−403.

(3) Wi, S. J.; Ji, N. R.; Park, K. Y. Synergistic biosynthesis of biphasic ethylene and reactive oxygen species in response to hemibiotrophic *Phytophthora parasitica* in tobacco plants. *Plant Physiol.* **2012**, *159*, 251−265.

(4) Bolwell, G. P.; Daudi, A. Reactive oxygen species in plant−pathogen interactions. In *Reactive Oxygen Species in Plant Signaling*; Rio, L. A., Puppo, A., Eds.; Springer: Berlin, Germany, 2009; pp 113−133.

(5) Wojtaszek, P. Oxidative burst: an early plant response to pathogen infection. *Biochem. J.* **1997**, *322* (3), 681−692.

(6) Alvarez, M. E.; Pennell, R. I.; Meijer, P. J.; Ishikawa, A.; Dixon, R. A.; Lamb, C. Reactive oxygen intermediates mediate a systemic signal network in the establishment of plant immunity. *Cell* **1998**, *92*, 773−784.

(7) Kobayashi, M.; Ohura, I.; Kawakita, K.; Yokota, N.; Fujiwara, M.; Shimamoto, K.; Doke, N.; Yoshioka, H. Calcium-dependent protein kinases regulate the production of reactive oxygen species by potato NADPH oxidase. *Plant Cell* **2007**, *19*, 1065−1080.

(8) Yoshioka, H.; Sugie, K.; Park, H. J.; Maeda, H.; Tsuda, N.; Kawakita, K.; Doke, N. Induction of plant gp91 phox homolog by fungal cell wall, arachidonic acid, and salicylic acid in potato. *Mol. Plant−Microbe Interact.* **2001**, *14*, 725−736.

(9) Torres, M. A. ROS in biotic interactions. *Physiol. Plant.* **2010**, *138*, 414−429.

(10) Yoshioka, H.; Bouteau, F.; Kawano, T. Discovery of oxidative burst in the field of plant immunity: looking back at the early pioneering works and towards the future development. *Plant Signaling Behav.* **2008**, *3*, 153−155.

(11) Apel, K.; Hirt, H. Reactive oxygen species: metabolism, oxidative stress, and signal transduction. *Annu. Rev. Plant Biol.* **2004**, *55*, 373−399.

(12) Mur, L. A.; Laarhoven, L. J.; Harren, F. J.; Hall, M. A.; Smith, A. R. Nitric oxide interacts with salicylate to regulate biphasic ethylene production during the hypersensitive response. *Plant Physiol.* **2008**, *148*, 1537−1546.

(13) Desikan, R.; A.-H.-Mackerness, S.; Hancock, J. T.; Neill, S. J. Regulation of the *Arabidopsis* transcriptome by oxidative stress. *Plant Physiol.* **2001**, *127*, 159−172.

(14) Vandenabeele, S.; Van Der Kelen, K.; Dat, J.; Gadjev, I.; Boonefaes, T.; Morsa, S.; Rottiers, P.; Slooten, L.; Van Montagu, M.; Zabeau, M.; Inze, D.; Van Breusegem, F. A comprehensive analysis of hydrogen peroxide-induced gene expression in tobacco. *Proc. Natl. Acad. Sci. U.S.A.* **2003**, *100*, 16113−16118.

(15) de Jong, A. J.; Yakimova, E. T.; Kapchina, V. M.; Woltering, E. J. A critical role for ethylene in hydrogen peroxide release during programmed cell death in tomato suspension cells. *Planta* **2002**, *214*, 537−545.

(16) Glazebrook, J. Contrasting mechanisms of defense against biotrophic and necrotrophic pathogens. *Annu. Rev. Phytopathol.* **2005**, *43*, 205−227.

(17) Dickman, M. B.; Park, Y. K.; Oltersdorf, T.; Li, W.; Clemente, T.; French, R. Abrogation of disease development in plants expressing animal antiapoptotic genes. *Proc. Natl. Acad. Sci. U.S.A.* **2001**, *98*, 6957−6962.

(18) Bollina, V.; Kumaraswamy, G. K.; Kushalappa, A. C.; Choo, T. M.; Dion, Y.; Rioux, S.; Faubert, D.; Hamzehzarghani, H. Mass spectrometry-based metabolomics application to identify quantitative resistance-related metabolites in barley against Fusarium head blight. *Mol. Plant Pathol.* **2010**, *11*, 769−782.

(19) Cho, K.; Kim, Y.; Wi, S. J.; Seo, J. B.; Kwon, J.; Chung, J. H.; Park, K. Y.; Nam, M. H. Nontargeted metabolite profiling in compatible pathogen-inoculated tobacco (*Nicotiana tabacum* L. cv. Wisconsin 38) using UPLC-Q-TOF/MS. *J. Agric. Food Chem.* **2012**, *60*, 11015−11028.

(20) Rieu, I.; Mariani, C.; Weterings, K. Expression analysis of five tobacco EIN3 family members in relation to tissue-specific ethylene responses. *J. Exp. Bot.* **2003**, *54*, 2239−2244.

(21) Iordachescu, M.; Verlinden, S. Transcriptional regulation of three EIN3-like genes of carnation (*Dianthus caryophyllus* L. cv. Improved White Sim) during flower development and upon wounding, pollination, and ethylene exposure. *J. Exp. Bot.* **2005**, *56*, 2011−2018.

(22) Gaquerel, E.; Heiling, S.; Schoettner, M.; Zurek, G.; Baldwin, I. T. Development and validation of a liquid chromatography-electrospray ionization-time-of-flight mass spectrometry method for induced changes in *Nicotiana attenuata* leaves during simulated herbivory. *J. Agric. Food Chem.* **2010**, *58*, 9418−9427.

(23) Shu, S.; Guo, S.-R.; Yuan, L.-Y. A review: Polyamines and photosynthesis. In *Advances in Photosynthesis − Fundamental Aspects*; Najafpour, M., Ed.; InTech: Rijeka, Croatia, 2012; pp 439−464.

(24) Yoo, T. H.; Park, C. J.; Ham, B. K.; Kim, K. J.; Paek, K. H. Ornithine decarboxylase gene (CaODC1) is specifically induced during TMV-mediated but salicylate-independent resistant response in hot pepper. *Plant Cell Physiol.* **2004**, *45*, 1537−1542.

(25) Yoda, H.; Hiroi, Y.; Sano, H. Polyamine oxidase is one of the key elements for oxidative burst to induce programmed cell death in tobacco cultured cells. *Plant Physiol.* **2006**, *142*, 193−206.

(26) Torrigiani, P.; Rabiti, A. L.; Bortolotti, C.; Betti, L.; Marani, F.; Canova, A.; Bagni, N. Polyamine synthesis and accumulation in the hypersensitive response to TMV in *Nicotiana tabacum*. *New Phytol.* **1997**, *135*, 467−473.

(27) Walters, D. R. Polyamines and plant disease. *Phytochemistry* **2003**, *64*, 97−107.

(28) Kaur, H.; Heinzel, N.; Schottner, M.; Baldwin, I. T.; Galis, I. R2R3-NaMYB8 regulates the accumulation of phenylpropanoid-

polyamine conjugates, which are essential for local and systemic defense against insect herbivores in *Nicotiana attenuata*. *Plant Physiol.* **2010**, *152*, 1731−1747.
(29) Onkokesung, N.; Gaquerel, E.; Kotkar, H.; Kaur, H.; Baldwin, I. T.; Galis, I. MYB8 controls inducible phenolamide levels by activating three novel hydroxycinnamoyl-coenzyme A:polyamine transferases in *Nicotiana attenuata*. *Plant Physiol.* **2012**, *158*, 389−407.
(30) Hagel, J. M.; Facchini, P. J. Elevated tyrosine decarboxylase and tyramine hydroxycinnamoyltransferase levels increase wound-induced tyramine-derived hydroxycinnamic acid amide accumulation in transgenic tobacco leaves. *Planta* **2005**, *221*, 904−914.
(31) Hagemeier, J.; Schneider, B.; Oldham, N. J.; Hahlbrock, K. Accumulation of soluble and wall-bound indolic metabolites in *Arabidopsis thaliana* leaves infected with virulent or avirulent *Pseudomonas syringae* pathovar tomato strains. *Proc. Natl. Acad. Sci. U.S.A.* **2001**, *98*, 753−758.
(32) Ishihara, A.; Kawata, N.; Matsukawa, T.; Iwamura, H. Induction of *N*-hydroxycinnamoyltyramine synthesis and tyramine *N*-hydroxycinnamoyltransferase (THT) activity by wounding in maize leaves. *Biosci., Biotechnol., Biochem.* **2000**, *64*, 1025−1031.
(33) Dow, M.; Newman, M. A.; von Roepenack, E. The induction and modulation of plant defense responses by bacterial lipopolysaccharides. *Annu. Rev. Phytopathol.* **2000**, *38*, 241−261.
(34) King, R. R.; Calhoun, L. A. A feruloyltyramine trimer isolated from potato common scab lesions. *Phytochemistry* **2010**, *71*, 2187−2189.
(35) Newman, M. A.; von Roepenack-Lahaye, E.; Parr, A.; Daniels, M. J.; Dow, J. M. Prior exposure to lipopolysaccharide potentiates expression of plant defenses in response to bacteria. *Plant J.* **2002**, *29*, 487−495.
(36) Howe, G. A.; Schilmiller, A. L. Oxylipin metabolism in response to stress. *Curr. Opin. Plant Biol.* **2002**, *5*, 230−236.
(37) Vellosillo, T.; Martinez, M.; Lopez, M. A.; Vicente, J.; Cascon, T.; Dolan, L.; Hamberg, M.; Castresana, C. Oxylipins produced by the 9-lipoxygenase pathway in *Arabidopsis* regulate lateral root development and defense responses through a specific signaling cascade. *Plant Cell* **2007**, *19*, 831−846.
(38) Vu, H. S.; Tamura, P.; Galeva, N. A.; Chaturvedi, R.; Roth, M. R.; Williams, T. D.; Wang, X.; Shah, J.; Welti, R. Direct infusion mass spectrometry of oxylipin-containing *Arabidopsis* membrane lipids reveals varied patterns in different stress responses. *Plant Physiol.* **2012**, *158*, 324−339.
(39) Sattler, S. E.; Mene-Saffrane, L.; Farmer, E. E.; Krischke, M.; Mueller, M. J.; DellaPenna, D. Nonenzymatic lipid peroxidation reprograms gene expression and activates defense markers in *Arabidopsis* tocopherol-deficient mutants. *Plant Cell* **2006**, *18*, 3706−3720.
(40) Buseman, C. M.; Tamura, P.; Sparks, A. A.; Baughman, E. J.; Maatta, S.; Zhao, J.; Roth, M. R.; Esch, S. W.; Shah, J.; Williams, T. D.; Welti, R. Wounding stimulates the accumulation of glycerolipids containing oxophytodienoic acid and dinor-oxophytodienoic acid in *Arabidopsis* leaves. *Plant Physiol.* **2006**, *142*, 28−39.
(41) Gobel, C.; Feussner, I.; Hamberg, M.; Rosahl, S. Oxylipin profiling in pathogen-infected potato leaves. *Biochim. Biophys. Acta* **2002**, *1584*, 55−64.
(42) Montillet, J. L.; Chamnongpol, S.; Rusterucci, C.; Dat, J.; van de Cotte, B.; Agnel, J. P.; Battesti, C.; Inze, D.; Van Breusegem, F.; Triantaphylides, C. Fatty acid hydroperoxides and H_2O_2 in the execution of hypersensitive cell death in tobacco leaves. *Plant Physiol.* **2005**, *138*, 1516−1526.
(43) Andersson, M. X.; Hamberg, M.; Kourtchenko, O.; Brunnstrom, A.; McPhail, K. L.; Gerwick, W. H.; Gobel, C.; Feussner, I.; Ellerstrom, M. Oxylipin profiling of the hypersensitive response in *Arabidopsis thaliana*. Formation of a novel oxo-phytodienoic acid-containing galactolipid, arabidopside E. *J. Biol. Chem.* **2006**, *281*, 31528−31537.